

---

# Can Generative Models Improve Self-Supervised Representation Learning?

---

Sana Ayromlou<sup>1</sup> Arash Afkanpour<sup>1</sup> Vahid Reza Khazaie<sup>1</sup> Fereshteh Forghani<sup>2</sup>

<sup>1</sup>Vector Institute <sup>2</sup>York University

sana.ayromlou@vectorinstitute.ai

arash.afkanpour@vectorinstitute.ai

vahidreza.khazaie@vectorinstitute.ai

forghani@yorku.ca

## Abstract

The rapid advancement in self-supervised learning (SSL) has highlighted its potential to leverage unlabeled data for learning rich visual representations. However, the existing SSL techniques, particularly those employing different augmentations of the same image, often rely on a limited set of simple transformations that are not representative of real-world data variations. This constrains the diversity and quality of samples, which leads to sub-optimal representations. In this paper, we introduce a novel framework that enriches the SSL paradigm by utilizing generative models to produce semantically consistent image augmentations. By directly conditioning generative models on a source image representation, our method enables the generation of diverse augmentations while maintaining the semantics of the source image, thus offering a richer set of data for self-supervised learning. Our extensive experimental results on various SSL methods demonstrate that our framework significantly enhances the quality of learned visual representations by up to 10% Top-1 accuracy in downstream tasks. This research demonstrates that incorporating generative models into the SSL workflow opens new avenues for exploring the potential of synthetic data. This development paves the way for more robust and versatile representation learning techniques.

## 1 Introduction

Self-supervised learning (SSL) is a machine learning approach where methods leverage large amounts of unlabeled data for representation learning. In the absence of any prior knowledge, most SSL methods assume that each data point is semantically different from other examples in a dataset. While this assumption can help devise a self-supervised representation learning algorithm, it is not sufficient to guarantee the generalization of representations to new tasks. As a result, some SSL methods rely on augmentation techniques (e.g., [Chen et al. \(2020\)](#); [He et al. \(2020\)](#); [Grill et al. \(2020\)](#)). These augmentations typically consist of a series of transformations, such as random crop, color jitter, or Gaussian blur, as shown in Fig. 1(a), which are used to define *positive labels* for the SSL task. These augmentations determine pixel-space changes that should result in similar embedding-space representations. Since these transformations specify what representations learn, a natural question is whether additional transformations improve the generalization and robustness of representations.

While some previous works have studied the impact of augmentations in representation learning (e.g., [Chen et al. \(2020\)](#), [Caron et al. \(2020\)](#)), until recently, this area has remained largely under-explored. More recently, new image transformations have been introduced in the context of self-supervised learning. For example, [Mansfield et al. \(2023\)](#) introduced random field transformations by applying local affine and color transformations whose parameters are specified by Gaussian random fields

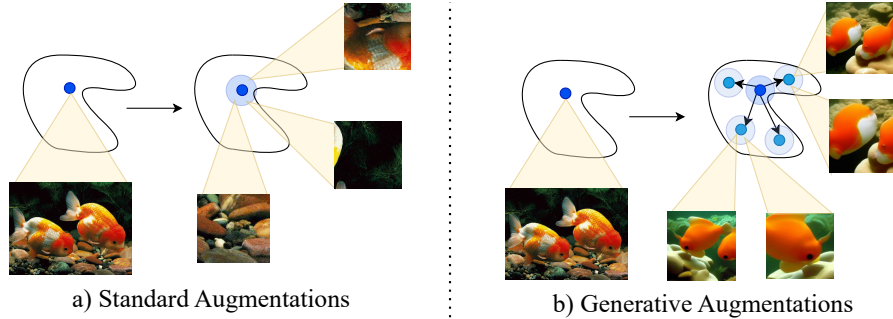


Figure 1: The effect of generative augmentation in enhancing diversity of views for joint-embedding SSL. Halos around each point show the effect of the standard augmentation in representation space. **a)** The standard SSL augmentations lack semantic diversity for effective representation learning. **b)** By generating instance-conditioned samples, and then applying the standard augmentations on top, we add more diversity in training data, leading to better representations.

(Adler et al., 2007). Rojas-Gomez et al. (2023) proposed style transfer as a form of transformation for SSL. While these works show that new transformations can improve representation learning, their transformations remain limited to certain predefined forms.

An important feature of SSL transformations is that while they transform an image in pixel space, they do not significantly modify its semantics. Guided by this view, we propose the notion of a *generalized transformation*, which satisfies these conditions: (1) the transformed image should be semantically similar to the original image, and (2) it should not make modifications that render the image unrealistic, which often happens by some of the standard transformations (e.g., color jitter). The question arises: given a source image, how can one generate transformed images that satisfy these conditions? For this task, we leverage instance-conditioned generative models. In particular, we study latent diffusion models (Rombach et al., 2022) and conditional Generative Adversarial Networks (GAN) (Casanova et al., 2021) that generate an output that is semantically similar to a source image. Our extensive empirical study in in-distribution and out-of-distribution cases demonstrates the effectiveness of our method for representation learning. The code to reproduce our empirical study is available at <https://anonymous.4open.science/r/genssl-121B>.

The key contributions of our work are as follows:

- We introduce a novel framework that leverages instance-conditioned generative models for generating semantically similar augmentations in self-supervised learning, advancing beyond the standard augmentation techniques.
- Our empirical results demonstrate the effectiveness of generative models to enhance the generalization and robustness of representations.
- By relying on instance-conditioned image generation, we eliminate the need for text-based image generation, as suggested in Tian et al. (2024). This enables the application of our method to datasets without a textual description, resulting in a more versatile and effective strategy for SSL training.

## 2 Background

### 2.1 Self-supervised learning

Self-supervised learning (SSL) leverages unlabeled data to create rich and generalizable representations. This approach offers numerous advantages due to its ability to train on extensive unlabeled data (Balestriero et al., 2023). A line of SSL methods, known as *joint embedding* methods, encourages two views of the same image, formed by augmentations such as cropping or color jitter, to be mapped to similar representations. This approach enables encoders to learn to differentiate the representation of each image, leading to decent linear separability. To prevent the encoders from collapsing by predicting a constant output for any input, various techniques are employed.

These methods, based on their objective functions or architectures, can be categorized as follows (Balestriero et al., 2023): 1) *Deep metric learning* methods originate from the concept of contrastive loss, which in an unsupervised manner, pulls representations of different transformed versions of the same image together while pushing representations of different images apart. **SimCLR** (Chen et al., 2020) uses the examples in each batch to calculate the contrastive loss. **MoCo** (He et al., 2020) is another method that learns an encoder by matching an encoded query to a dictionary of encoded keys using contrastive loss. 2) *Self-distillation* methods rely on a straightforward mechanism of feeding two different views to two encoders and mapping one to the other using a predictor (Zhou et al., 2021; Caron et al., 2021; Oquab et al., 2023). They prevent collapse by introducing asynchrony in updating the encoders. **BYOL** (Grill et al., 2020) first introduced self-distillation as a means to avoid collapse. **SimSiam** (Chen and He, 2021) replaces the BYOL moving average encoder with a stop-gradient mechanism. 3) *Canonical correlation analysis* methods originate from the Canonical Correlation Framework (CCA) (Hotelling, 1992; Caron et al., 2018; Bardes et al., 2021). At a high level CCA aims to infer the relationship between variables by analyzing the covariance matrix. **Barlow Twins** (Zbontar et al., 2021) uses cross-correlation of the embedding features to achieve self-supervised learning goals. In this paper, we evaluate the effectiveness of our proposed generative augmentation when integrated into the augmentation pipeline of the highlighted techniques (in bold).

## 2.2 Generative methods

*Generative Adversarial Networks* (GAN) (Goodfellow et al., 2014) have significantly advanced the field of image generation. Recently, there have been some works on conditioning GANs over a feature vector (Mangla et al., 2022; Casanova et al., 2021). In this work, we chose Instance-Conditioned GANs (ICGAN) (Casanova et al., 2021), which innovatively extends this framework by conditioning the generation and discrimination processes on a specific image. ICGAN aims to model the data distribution as a mixture of local densities around each instance, utilizing representations of these instances as additional input to both generator and discriminator. This conditioning allows the model to generate images that are semantically similar to a given instance. Such an approach addresses the optimization difficulties and mode collapse issues prevalent in traditional GANs by ensuring a more focused generation process. This method can be leveraged to create semantically consistent augmentations for SSL.

*Diffusion Models*, a class of likelihood-based generative models, have gained attention for their ability to generate high-quality images (Dhariwal and Nichol, 2021; Ho et al., 2020; Nichol and Dhariwal, 2021). They work by gradually reducing noise from an image, with their training objective expressed as a re-weighted variational lower-bound (Ho et al., 2020). Despite their ability to generate high-quality images, due to their incremental noise reduction process, these models have traditionally faced challenges of long training and inference times. While inference challenges can be mitigated with advanced sampling strategies (Salimans and Ho, 2022; Song et al., 2020) and hierarchical approaches (Ho et al., 2022), training on high-resolution image data remains computationally expensive. To address this, latent diffusion models (LDM) have been introduced (Rombach et al., 2022). These models operate in a latent space with lower dimensionality than the input space, making training computationally cheaper, and speeding up inference with almost no reduction in synthesis quality. They also introduced cross-attention layers into the model architecture, where various conditioning inputs, such as text, images, or other representations, can be applied to get a conditional output. The conditional LDM,  $\epsilon_\theta$ , which is usually a UNet (Ronneberger et al., 2015), and a domain-specific encoder,  $\phi_\tau$ , that provides the conditioning vector, are learned jointly by optimizing,

$$\theta^*, \tau^* = \arg \min_{\theta, \tau} \mathbb{E}_{\epsilon \sim \mathcal{N}(0, I), t, y} [\|\epsilon - \epsilon_\theta(z_t, t, \phi_\tau(y))\|_2^2],$$

where  $t$  is the timestep parameter,  $z_t$  is the noisy latent vector at timestep  $t$ , and  $y$  is the conditioning input (e.g. a text prompt). Given their ability to generate high-quality diverse samples, diffusion models stand out as a compelling option for our new generative augmentation.

## 3 Generative self-supervised learning

Joint embedding SSL methods create two or more views by applying a series of transformations to an image. More formally, given a batch of images,  $\mathcal{B} = \{x_1, \dots, x_N\}$ , joint embedding SSL methods

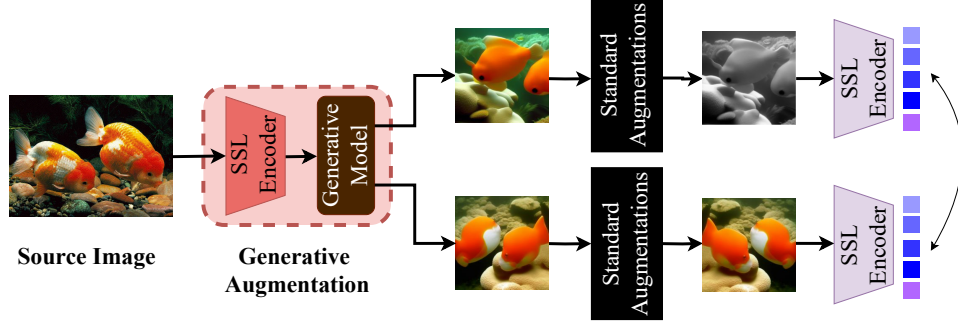


Figure 2: Our augmentation pipeline utilizes generative models, i.e., Stable Diffusion or ICGAN, conditioned on the source image representation, accompanied by the standard SSL augmentations. The components inside the *Generative Augmentation* module, i.e. the pretrained SSL encoder and the generative model remain frozen throughout the SSL training process.

learn an encoder,  $f_\theta$ , by optimizing a loss function,  $\mathcal{L}$ , over the batch,  $\mathcal{B}$ :

$$\theta^*, \psi^* = \arg \min_{\theta, \psi} \mathbb{E}_{A_1, A_2, \mathcal{B}} \left[ \mathcal{L} \left( g_\psi \left( f_\theta \left( A_1(\mathcal{B}) \right) \right), g_\psi \left( f'_\theta \left( A_2(\mathcal{B}) \right) \right) \right) \right],$$

where  $A_1$  and  $A_2$  are augmentations applied to the images in  $\mathcal{B}$  to create two views of each image,  $g_\psi$  is a projection/prediction head applied to the output of the encoder before calculating the loss, and  $f'$  is a variant of  $f$  that, depending on the SSL algorithm, could be for instance, identical to  $f$  (SimCLR), its exponential moving average (MoCo), or its frozen version (SimSiam).

The augmentations,  $A_1$  and  $A_2$ , are a series of  $K$  sequentially-applied transformations,  $A_j = T_K^{\gamma_K} \circ \dots \circ T_1^{\gamma_1}$ , where  $T_i^{\gamma_i}$  is parameterized by  $\gamma_i$ . For example, a crop transformation could be parameterized by crop area, aspect ratio, etc. While parameterization of transformations increases the versatility of the views, they are often limited in producing semantically meaningful variations of the data. For example, previous SSL methods apply transformations such as random crop, color jitter, horizontal flip, grayscale (color removal), and Gaussian blur. Adding transformations that create more diversity in the output of the augmentation pipeline could potentially improve the generalization of learned representations.

As illustrated in Fig. 1, standard transformations might not adequately represent the intrinsic variability found in real-world data, and may alter the semantic meaning of the input. For example, the color jitter transformation might lead to color changes that render an image unrealistic.

To overcome these limitations, we expand SSL transformations with the introduction of a novel non-parametric transformation that is capable of producing diverse, realistic images that follow the distribution of real-world data. The only constraint is that to learn useful representations, a transformed image must remain semantically similar to its source image.

As illustrated in Fig. 2, the foundation of our novel transformation lies in conditional generative models. These models, such as conditional latent diffusion models (Rombach et al., 2022; Bordes et al., 2021), instance-conditioned GANs (Casanova et al., 2021), and conditional Variational Autoencoders (cVAEs) (Zhang et al., 2021) enable the generation of images based on specific input data. By conditioning the generation process on the input, the model ensures that the semantics of the original image is preserved to a large extent. Moreover, the use of conditional generative models allows for a more nuanced augmentation process, where the generated samples closely follow the distribution of real images while exhibiting variations that enhance the diversity of the training data for self-supervised learning. Our new transformation is denoted by:

$$T_0(x) = \begin{cases} G(z; \phi(x)) & \text{if } p \leq p_0 \\ x & \text{otherwise,} \end{cases}$$

where  $G$  denotes a conditional generative model,  $z \sim \mathcal{N}(0, I)$  is a noise vector,  $\phi$  is a pretrained encoder, such as a CLIP image encoder (Radford et al., 2021), that provides the condition vector for the generative model,  $p \in [0, 1]$  is a random number, and  $p_0$  is a parameter specifying the probability of applying the generative augmentation.

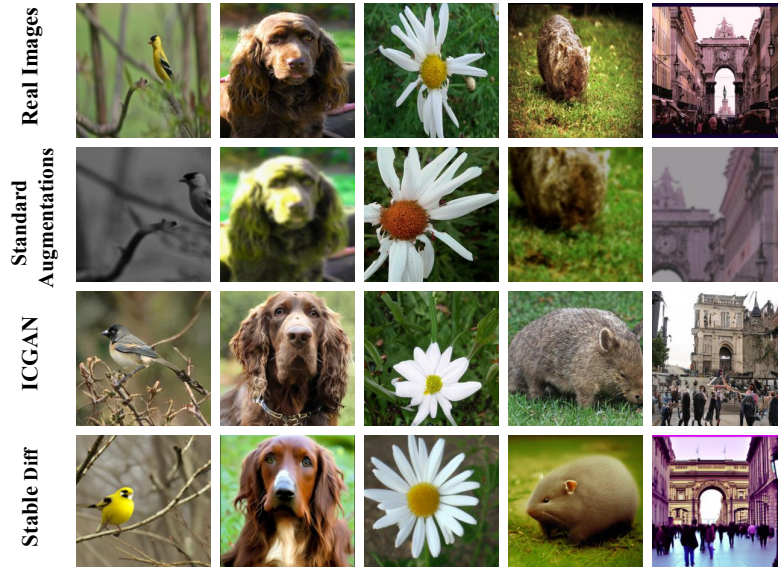


Figure 3: Examples of various augmentations show that while standard augmentations (second row) often lack diversity, instance-based generative augmentations are capable of producing diverse and realistic images that preserve the semantics of the original image.

Note that, unlike StableRep (Tian et al., 2024), we do not replace a real dataset with a synthetic one. Instead, we leverage conditional generative models to enrich augmentations for self-supervised learning. Another distinction is that our method does not require text prompts and directly uses images as input to the generative model.

## 4 Empirical study

### 4.1 Setup

Utilizing the Solo-learn library (Da Costa et al., 2022), we evaluate the proposed generative augmentation across five joint-embedding SSL techniques: SimCLR (Chen et al., 2020), SimSiam (Chen and He, 2021), BYOL (Grill et al., 2020), Barlow Twins (Zbontar et al., 2021), and MoCo (He et al., 2020). We pretrain a ResNet50 encoder using these SSL techniques for 100 epochs on the ImageNet training split. For evaluation, we follow the linear probing protocol of previous works by training a linear classifier on the output of the frozen encoder. Our downstream tasks are image classification on the ImageNet (Deng et al., 2009), Food 101 (Bossard et al., 2014), Places 365 (Zhou et al., 2017), iNaturalist 2018 (Van Horn et al., 2018), CIFAR 10, and CIFAR 100 (Krizhevsky et al., 2009) datasets. For all datasets, except for Places 365, a linear classifier is trained on the corresponding training split for 100 epochs. For Places 365, training is performed for 45 epochs. After training the linear classifier, we evaluate the classifier on the corresponding validation set.

In the following experiments, *Baseline* refers to the model that uses standard augmentations to create the views. The sequence of transformations to create each view is as follows: (1) random crop with the relative crop area selected randomly from  $[0.2, 1]$ , (2) scale to  $224 \times 224$ , (3) color jitter, (4) grayscale, (5) Gaussian blur, (6) horizontal flip. Each augmentation is applied stochastically with a probability value, as detailed in the Section A of Appendix. For our method, we prepend the above sequence with a generative augmentation that takes a source image and, depending on the experiment, uses either Stable Diffusion, which is a conditional latent diffusion model, or ICGAN, to return a synthetic image as described in Section 3. To accelerate training, instead of generating synthetic images on-the-fly, we generate 10 images per each image in the ImageNet training set offline, and load them during SSL training. Unless specified otherwise, we apply the generative augmentation to create one view of the source image with probability  $p = 1$ , while the other view is created with the standard augmentations. Our reasoning for this approach was to ensure fidelity to the original images

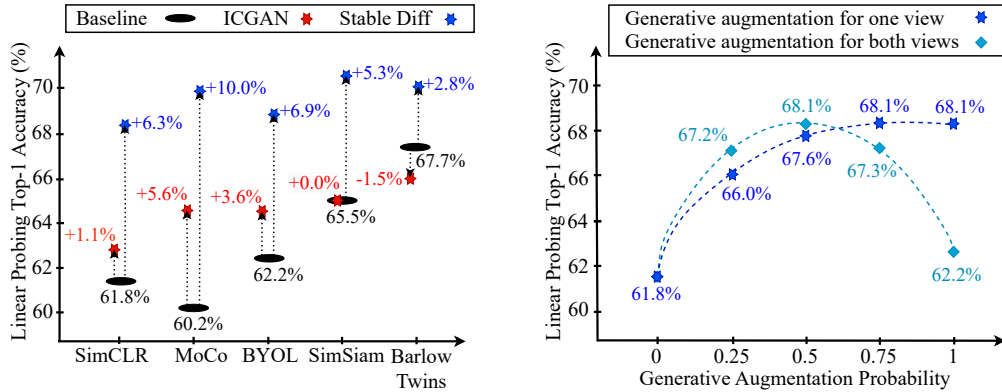


Figure 4: Linear probing Top-1 accuracy on ImageNet validation set. **Left:** Improvement obtained by generative augmentations with Stable Diffusion and ICGAN across five SSL techniques. **Right:** The effect of different probability values of applying the generative augmentation.

in SSL training and to avoid having both views be synthetic. Later we will also study the effect of applying the synthetic augmentation to create both views.

## 4.2 Results

We frame our experiments to answer four research questions about our proposed generative augmentation technique.

**RQ1: Does the generative transformation improve visual representation learning consistently across different SSL techniques?** We evaluate the effectiveness of the generative transformation across five SSL techniques. We compare an augmentation pipeline that includes the generative transformation obtained by either Stable Diffusion (Stable Diff) or ICGAN against the Baseline, which refers to pretraining the SSL encoder with only the standard augmentations. Fig. 4 (left) shows the linear probing Top-1 accuracy for different SSL techniques. For Top-5 accuracy results, please refer to Table 9 in the Appendix. Across all techniques, the addition of a generative transformation via Stable Diffusion consistently improves representation learning, which in turn enhances downstream classification accuracy between 3% to 10%. With the exception of Barlow Twins, we observe a similar trend with generative augmentations generated by ICGAN. However, the magnitude of improvement is smaller compared to Stable Diffusion. We conjecture that this is because the quality and diversity of images generated by Stable Diffusion better reflect the distribution of real images compared to those generated by ICGAN, as depicted by some examples in Fig. 3. These factors are often determined by the size of the model and the volume of pretraining data. Stable Diffusion is a larger model and has been trained on LAION-400M which contains 400 million images (Rombach et al., 2022), while ICGAN was trained on ImageNet with 1.2 million images.

To measure out-of-distribution performance of learned representations, we evaluate these models across other downstream classification tasks. Table 1 shows the Top-1 accuracy results. In line with the above results on ImageNet, the Stable Diffusion generative transformation outperforms other baselines across all datasets. ICGAN, with the exception of a few cases, also outperforms the baseline, but we observe larger improvement with Stable Diffusion compared to ICGAN. These results, along with the in-distribution results, indicate that the generative transformation consistently improves representation learning across different SSL techniques.

**RQ2: What probability of applying the generative augmentation achieves the best visual representations?** Each image transformation in the standard augmentations is applied with a certain probability value tuned to achieve the best visual representations. While higher probability values create more diversity in augmentations, they could potentially hinder fidelity or create undesirable artifacts that result in sub-optimal representations.

For this experiment we used Stable Diffusion for synthetic image generation and applied the new augmentation with probability  $p \in \{0, 0.25, 0.5, 0.75, 1\}$  to one view. We then trained a SimCLR

Table 1: Top-1 accuracy (%) results of linear probing on several datasets with different augmentation strategies. Numbers inside parentheses show the absolute percentage difference from the baseline.

		<b>Food101</b>	<b>CIFAR10</b>	<b>CIFAR100</b>	<b>Places365</b>	<b>iNaturalist2018</b>
<b>SimCLR</b>	Baseline	58.03	61.74	36.88	46.11	20.17
	ICGAN	57.42 (-0.61)	61.92 (+0.18)	39.45 (+2.57)	45.75 (-0.36)	20.25 (+0.08)
	Stable Diff	61.78 (+3.75)	63.19(+1.45)	39.60 (+2.72)	48.40 (+2.29)	24.08 (+3.91)
<b>MoCo</b>	Baseline	54.50	58.17	34.28	45.70	16.52
	ICGAN	59.92 (+5.42)	64.48 (+7.31)	40.57 (+6.29)	47.69 (+1.99)	21.90 (+5.38)
	Stable Diff	62.79 (+8.29)	64.62 (+7.45)	41.33 (+7.05)	49.26 (+3.56)	25.20 (+8.68)
<b>BYOL</b>	Baseline	54.14	55.34	28.70	46.93	6.91
	ICGAN	53.35 (-0.79)	60.20 (+4.86)	35.17 (+6.47)	46.84 (-0.09)	8.96 (+2.05)
	Stable Diff	55.22 (+1.08)	60.30 (+4.96)	36.24 (+7.54)	47.71 (+0.78)	9.96 (+3.05)
<b>SimSiam</b>	Baseline	60.71	61.93	37.69	48.78	22.07
	ICGAN	61.06 (+0.36)	63.68 (+1.75)	38.85 (+1.16)	47.41 (-1.37)	23.13 (+1.06)
	Stable Diff	67.97 (+7.26)	64.38 (+2.45)	41.31 (+3.62)	49.95 (+1.17)	31.47 (+9.4)
<b>Barlow Twins</b>	Baseline	66.71	65.49	41.19	49.47	27.99
	ICGAN	64.98 (-1.73)	64.95 (-0.46)	41.52 (+0.33)	47.98 (-1.49)	25.86 (-2.13)
	Stable Diff	68.62 (+1.91)	65.21 (-0.28)	41.91 (+0.72)	49.66 (+0.19)	31.14 (+3.15)

encoder with each value of  $p$ , and compared these encoders with linear probing on the ImageNet validation split. The dark blue curve in Fig. 4 (right) shows the Top-1 accuracy results for different  $p$  values. The results show a monotonic increase in the quality of visual representations as  $p$  increases with  $p = 0.75$  and  $p = 1$  achieving the best results. These results show the effectiveness of the new augmentation for representation learning.

In addition, we applied the generative augmentation with the above probability values to *both* views of the source image. The results are shown as the light blue curve in Fig. 4 (right). In this case,  $p = 0.5$  achieves the best visual representations, as it strikes a balance between real and synthetic images in the views. However, increasing the probability of the generative augmentation beyond that will degrade performance as it likely creates excessive deviation from the original data. Note, however, that  $p = 1$  still outperforms no generative augmentation ( $p = 0$ ), indicating the effectiveness of the new augmentation.

**RQ3: Considering that the new generative augmentation employs a conditional generative process dependent on a pretrained encoder, does self-supervised learning with this transformation produce the same latent-space data distribution as the pretrained encoder?**

This question is crucial because our augmentation technique relies on conditional image generation using a pretrained encoder for image conditioning (e.g., a pretrained CLIP encoder for Stable Diffusion). If the distributions of representation vectors are identical or very similar, the new data augmentation would offer little to no advantage for representation learning, as such representations are already accessible through the pretrained SSL encoder. Note that in this case we cannot rely on downstream accuracy for two reasons: (1) comparing downstream accuracy of two encoders provides little insight into the similarity of their representation spaces, (2) the CLIP encoder is trained on 400 million image-text pairs (Radford et al., 2021), which is significantly larger than the ImageNet training split (1.2 million images) used for training our SSL encoders, rendering any downstream accuracy comparison unfair. Instead, to compare representations of different encoders we employ two dissimilarity measures, i.e. Centered Kernel Alignment (CKA) (Kornblith et al., 2019) and Orthogonal Procrustes Distance (OPD) (Ding et al., 2021), which have been used to compare representations between layers of a network or between different trained models. Let  $\mathcal{D} = \{x_i\}_{i=1}^N$  be a dataset of  $N$  examples, where each example  $x_i \in \mathbb{R}^s$ . Let  $f_A : \mathbb{R}^s \rightarrow \mathbb{R}^p$  and  $f_B : \mathbb{R}^s \rightarrow \mathbb{R}^q$  denote two encoders. Let  $A \in \mathbb{R}^{p \times N}$  and  $B \in \mathbb{R}^{q \times N}$  denote the representation matrices obtained by

Table 2: CKA and OPD dissimilarity values between different representation pairs. We report the mean and 95% bootstrap confidence intervals over 100 runs.

Representation Pair	CKA	OPD
(SimCLR <sub>1</sub> , SimCLR <sub>2</sub> )	0.395 ± 0.006	0.022 ± 0.001
(SimCLR <sub>1</sub> , CLIP)	0.964 ± 0.002	0.580 ± 0.002
(SimCLR <sub>2</sub> , CLIP)	0.952 ± 0.002	0.574 ± 0.002

applying  $f_A$  and  $f_B$  to data points in  $\mathcal{D}$  respectively. The dissimilarity measure based on CKA is defined by,

$$d_{\text{CKA}}(A, B) = 1 - \frac{\|AB^\top\|_F^2}{\|AA^\top\|_F\|BB^\top\|_F}.$$

The OPD dissimilarity measure is the solution to the following optimization problem:

$$d_{\text{OPD}}(A, B) = \min_R \|B - RA\|_F^2, \quad \text{s.t. } R^\top R = \mathbb{I}.$$

Here,  $\|\cdot\|_F$  denotes Frobenius norm and  $\mathbb{I}$  is the identity matrix. Per standard practice, we normalize each matrix by first centering the features around the origin, then dividing by the Frobenius norm of the matrix before calculating these measures.

For this analysis, we measure the dissimilarity of representations between CLIP (the encoder used for conditioning Stable Diffusion) and SimCLR encoders trained with our generative transformation. We use the ImageNet validation set as data points to build the representation matrices. Since  $d_{\text{CKA}}$  and  $d_{\text{OPD}}$  are measured between two sets, we first require to establish a baseline for dissimilarity value between two sets of similar representations so we can compare other values against it. For this purpose we trained two SimCLR encoders with different weight initialization. While we acknowledge that the representation spaces of these models might not be identical, the dissimilarity value between them can be used as a baseline for comparing other values. Table 2 presents the dissimilarity values between different encoders. Dissimilarity values between the SimCLR encoders measured by both CKA and OPD are significantly smaller than the values between each SimCLR encoder and the CLIP encoder. These results demonstrate that the representations of SimCLR trained with the generative transformation are different from the representations of CLIP. In other words, representation learning with the proposed generative transformation does not trivially yield the same representation space of the pretrained encoder of the generative process.

**RQ4: Can we replace the standard augmentations with the generative augmentation for self-supervised learning?** Previous work on SSL augmentations has focused on enhancing the diversity of augmentations by adding new transformations to the pipeline. To the best of our knowledge, no attempt has been made to replace the standard augmentations with a new one, as it could significantly reduce the diversity of views and result in poor representations. Notably, Tian et al. (2024) observed that contrastive learning with a limited number of synthetic images benefits from the standard augmentations, as they help reduce overfitting. We investigate whether the new augmentation can replace the standard augmentations and whether keeping the standard augmentations in the pipeline is still beneficial for visual representation learning.

For this study we trained SimCLR models with different augmentation strategies and compared their representations by linear probing on the ImageNet validation set. Here, *Baseline* refers to the standard augmentations (crop and resize, color jitter, grayscale, Gaussian blur, and horizontal flip), and *Only generative* refers to using only the new generative augmentation obtained from Stable Diffusion. We also included another strategy, namely *Generative & Random Crop* that applies the generative transformation, followed by the random crop transformation. We particularly chose random crop as Chen et al. (2020) noted that this is the most effective augmentation among the standard ones. Similar to the previous experiments, in this case the generative augmentation is applied to only one view. However, changes to the standard augmentations, including removing them altogether in the *Only generative* strategy, apply to both views. For completeness, we included *Generative & Standard* in the results, which applies the generative augmentation followed by the standard augmentations. Table 3 shows the Top-1 accuracy of these models. The model trained with only the generative augmentation outperforms the standard SSL augmentations by 2%, demonstrating the effectiveness of the new transformation in creating diverse views for SSL training. Other strategies, i.e. Generative & Random



Table 3: The effect of different augmentation strategies on representation learning, measured by downstream Top-1 accuracy on the ImageNet validation set. Numbers inside parentheses show the absolute percentage difference from the baseline.

Augmentation Strategy	Top-1 Accuracy
Baseline (only standard augmentations)	61.84
Only generative	63.80 (+1.96)
Generative & Random Crop	67.15 (+5.31)
Generative & Standard	68.11 (+6.27)

Crop and Generative & Standard, achieve higher downstream accuracy, indicating that the standard augmentations are still beneficial for visual representation learning.

## 5 Related work

With the advance of generative models, the use of synthetic data has become a tool for training better models in various domains. In computer vision, synthetic data has been utilized to enhance model performance in tasks such as object detection (Lin et al., 2023), semantic segmentation (Chen et al., 2019; Ros et al., 2016), and classification (Azizi et al., 2023; Sariyildiz et al., 2023). In representation learning, synthetic data has been leveraged for multi-task learning (Ren and Lee, 2018), and manipulating latent data representation (Liu et al., 2022; Baradad Jurjo et al., 2021; Jahanian et al., 2021). Jahanian et al. (2021) investigated learning visual representations from synthetic data generated by black-box models, emphasizing the ability of latent space transformations to facilitate contrastive learning and improve performance through careful sampling and training methods. It highlights generative models as a compact alternative to traditional datasets, predicting a shift towards reliance on model-generated data. The works of Donahue et al. (2016); Donahue and Simonyan (2019) introduce Bidirectional Generative Adversarial Networks (BiGAN) and BigBiGAN, which incorporate an inverse mapping mechanism within the GAN framework to enable both forward and inverse mappings between latent space and data. This allows for capturing semantic variations more effectively and making the representations valuable for auxiliary tasks. More recently, StableRep (Tian et al., 2024) showed how visual representations learned from synthetic text-to-image data can be more effective than representations learned by using only real images in various downstream tasks.

## 6 Conclusion, limitations, and broader impact

Image augmentation is a crucial component of joint embedding self-supervised learning. While many techniques rely on a limited set of transformations, recently, a few studies have proposed new parametric pixel-space transformations to enhance augmentations. In this paper, we introduced a new generalized augmentation method that leverages instance-conditioned generative models to transform an image while preserving its semantics. Our empirical study demonstrates the effectiveness of the generative augmentations for self-supervised representation learning.

Our method currently relies on pretrained generative models. An interesting direction to expand this work is to co-train the instance-conditioned generative model and the SSL encoder simultaneously. While care must be taken to avoid a possible collapse to trivial solutions, this approach could potentially lead to enhanced generative models for the SSL task.

**Broader impact.** Our method illustrates the potential for improving visual representation learning through the use of synthetic data generated by pretrained generative models. Since generating synthetic data is less costly and more feasible than collecting real data, this approach can improve model performance in domains with limited data by expanding the available training datasets. However, we also recognize the risk that pretrained generative models, which may have been trained on biased datasets, could propagate and even amplify these biases in applications that rely on synthetic data.

## References

- Adler, R. J., Taylor, J. E., et al. (2007). *Random fields and geometry*, volume 80. Springer.
- Azizi, S., Kornblith, S., Saharia, C., Norouzi, M., and Fleet, D. J. (2023). Synthetic data from diffusion models improves imagenet classification. *arXiv preprint arXiv:2304.08466*.
- Balestriero, R., Ibrahim, M., Sobal, V., Morcos, A., Shekhar, S., Goldstein, T., Bordes, F., Bardes, A., Mialon, G., Tian, Y., et al. (2023). A cookbook of self-supervised learning. *arXiv preprint arXiv:2304.12210*.
- Baradad Jurjo, M., Wulff, J., Wang, T., Isola, P., and Torralba, A. (2021). Learning to see by looking at noise. *Advances in Neural Information Processing Systems*, 34:2556–2569.
- Bardes, A., Ponce, J., and LeCun, Y. (2021). Vicreg: Variance-invariance-covariance regularization for self-supervised learning. *arXiv preprint arXiv:2105.04906*.
- Bordes, F., Balestriero, R., and Vincent, P. (2021). High fidelity visualization of what your self-supervised representation knows about. *arXiv preprint arXiv:2112.09164*.
- Bossard, L., Guillaumin, M., and Van Gool, L. (2014). Food-101—mining discriminative components with random forests. In *Computer Vision—ECCV 2014: 13th European Conference, Zurich, Switzerland, September 6–12, 2014, Proceedings, Part VI 13*, pages 446–461. Springer.
- Caron, M., Bojanowski, P., Joulin, A., and Douze, M. (2018). Deep clustering for unsupervised learning of visual features. In *Proceedings of the European conference on computer vision (ECCV)*, pages 132–149.
- Caron, M., Misra, I., Mairal, J., Goyal, P., Bojanowski, P., and Joulin, A. (2020). Unsupervised learning of visual features by contrasting cluster assignments. *Advances in neural information processing systems*, 33:9912–9924.
- Caron, M., Touvron, H., Misra, I., Jégou, H., Mairal, J., Bojanowski, P., and Joulin, A. (2021). Emerging properties in self-supervised vision transformers. In *Proceedings of the IEEE/CVF international conference on computer vision*, pages 9650–9660.
- Casanova, A., Careil, M., Verbeek, J., Drozdal, M., and Romero Soriano, A. (2021). Instance-conditioned gan. *Advances in Neural Information Processing Systems*, 34:27517–27529.
- Chen, T., Kornblith, S., Norouzi, M., and Hinton, G. (2020). A simple framework for contrastive learning of visual representations. In *International conference on machine learning*, pages 1597–1607. PMLR.
- Chen, X. and He, K. (2021). Exploring simple siamese representation learning. In *Proceedings of the IEEE/CVF conference on computer vision and pattern recognition*, pages 15750–15758.
- Chen, Y., Li, W., Chen, X., and Gool, L. V. (2019). Learning semantic segmentation from synthetic data: A geometrically guided input-output adaptation approach. In *Proceedings of the IEEE/CVF conference on computer vision and pattern recognition*, pages 1841–1850.
- Da Costa, V. G. T., Fini, E., Nabi, M., Sebe, N., and Ricci, E. (2022). solo-learn: A library of self-supervised methods for visual representation learning. *Journal of Machine Learning Research*, 23(56):1–6.
- Deng, J., Dong, W., Socher, R., Li, L.-J., Li, K., and Fei-Fei, L. (2009). Imagenet: A large-scale hierarchical image database. In *2009 IEEE conference on computer vision and pattern recognition*, pages 248–255. Ieee.
- Dhariwal, P. and Nichol, A. (2021). Diffusion models beat gans on image synthesis. *Advances in neural information processing systems*, 34:8780–8794.
- Ding, F., Denain, J.-S., and Steinhardt, J. (2021). Grounding representation similarity with statistical testing. *arXiv preprint arXiv:2108.01661*.

- Donahue, J., Krähenbühl, P., and Darrell, T. (2016). Adversarial feature learning. *arXiv preprint arXiv:1605.09782*.
- Donahue, J. and Simonyan, K. (2019). Large scale adversarial representation learning. *Advances in neural information processing systems*, 32.
- Goodfellow, I., Pouget-Abadie, J., Mirza, M., Xu, B., Warde-Farley, D., Ozair, S., Courville, A., and Bengio, Y. (2014). Generative adversarial nets. *Advances in neural information processing systems*, 27.
- Grill, J.-B., Strub, F., Alché, F., Tallec, C., Richemond, P., Buchatskaya, E., Doersch, C., Avila Pires, B., Guo, Z., Gheshlaghi Azar, M., et al. (2020). Bootstrap your own latent—a new approach to self-supervised learning. *Advances in neural information processing systems*, 33:21271–21284.
- He, K., Fan, H., Wu, Y., Xie, S., and Girshick, R. (2020). Momentum contrast for unsupervised visual representation learning. In *Proceedings of the IEEE/CVF conference on computer vision and pattern recognition*, pages 9729–9738.
- Ho, J., Jain, A., and Abbeel, P. (2020). Denoising diffusion probabilistic models. *Advances in neural information processing systems*, 33:6840–6851.
- Ho, J., Saharia, C., Chan, W., Fleet, D. J., Norouzi, M., and Salimans, T. (2022). Cascaded diffusion models for high fidelity image generation. *The Journal of Machine Learning Research*, 23(1):2249–2281.
- Hotelling, H. (1992). Relations between two sets of variates. In *Breakthroughs in statistics: methodology and distribution*, pages 162–190. Springer.
- Jahanian, A., Puig, X., Tian, Y., and Isola, P. (2021). Generative models as a data source for multiview representation learning. *arXiv preprint arXiv:2106.05258*.
- Kornblith, S., Norouzi, M., Lee, H., and Hinton, G. (2019). Similarity of neural network representations revisited. In *International conference on machine learning*, pages 3519–3529. PMLR.
- Krizhevsky, A., Hinton, G., et al. (2009). Learning multiple layers of features from tiny images.
- Lin, S., Wang, K., Zeng, X., and Zhao, R. (2023). Explore the power of synthetic data on few-shot object detection. In *Proceedings of the IEEE/CVF Conference on Computer Vision and Pattern Recognition (CVPR) Workshops*, pages 638–647.
- Liu, H., Zahavy, T., Mnih, V., and Singh, S. (2022). Palm up: Playing in the latent manifold for unsupervised pretraining. *Advances in Neural Information Processing Systems*, 35:35880–35893.
- Mangla, P., Kumari, N., Singh, M., Krishnamurthy, B., and Balasubramanian, V. N. (2022). Data instance prior (disp) in generative adversarial networks. In *Proceedings of the IEEE/CVF Winter Conference on Applications of Computer Vision*, pages 451–461.
- Mansfield, P. A., Afkanpour, A., Morningstar, W. R., and Singhal, K. (2023). Random field augmentations for self-supervised representation learning. *arXiv preprint arXiv:2311.03629*.
- Nichol, A. Q. and Dhariwal, P. (2021). Improved denoising diffusion probabilistic models. In *International Conference on Machine Learning*, pages 8162–8171. PMLR.
- Oquab, M., Darcet, T., Moutakanni, T., Vo, H., Szafraniec, M., Khalidov, V., Fernandez, P., Haziza, D., Massa, F., El-Nouby, A., et al. (2023). Dinov2: Learning robust visual features without supervision. *arXiv preprint arXiv:2304.07193*.
- Radford, A., Kim, J. W., Hallacy, C., Ramesh, A., Goh, G., Agarwal, S., Sastry, G., Askell, A., Mishkin, P., Clark, J., et al. (2021). Learning transferable visual models from natural language supervision. In *International conference on machine learning*, pages 8748–8763. PMLR.
- Ren, Z. and Lee, Y. J. (2018). Cross-domain self-supervised multi-task feature learning using synthetic imagery. In *Proceedings of the IEEE conference on computer vision and pattern recognition*, pages 762–771.

- Rojas-Gomez, R. A., Singhal, K., Etemad, A., Bijamov, A., Morningstar, W. R., and Mansfield, P. A. (2023). Sssl: Enhancing self-supervised learning via neural style transfer. *arXiv preprint arXiv:2312.01187*.
- Rombach, R., Blattmann, A., Lorenz, D., Esser, P., and Ommer, B. (2022). High-resolution image synthesis with latent diffusion models. In *Proceedings of the IEEE/CVF conference on computer vision and pattern recognition*, pages 10684–10695.
- Ronneberger, O., Fischer, P., and Brox, T. (2015). U-net: Convolutional networks for biomedical image segmentation. In *Medical image computing and computer-assisted intervention–MICCAI 2015: 18th international conference, Munich, Germany, October 5-9, 2015, proceedings, part III 18*, pages 234–241. Springer.
- Ros, G., Sellart, L., Materzynska, J., Vazquez, D., and Lopez, A. M. (2016). The synthia dataset: A large collection of synthetic images for semantic segmentation of urban scenes. In *Proceedings of the IEEE conference on computer vision and pattern recognition*, pages 3234–3243.
- Salimans, T. and Ho, J. (2022). Progressive distillation for fast sampling of diffusion models. *arXiv preprint arXiv:2202.00512*.
- Sariyildiz, M. B., Alahari, K., Larlus, D., and Kalantidis, Y. (2023). Fake it till you make it: Learning transferable representations from synthetic imagenet clones. In *CVPR 2023–IEEE/CVF Conference on Computer Vision and Pattern Recognition*.
- Song, J., Meng, C., and Ermon, S. (2020). Denoising diffusion implicit models. *arXiv preprint arXiv:2010.02502*.
- Tian, Y., Fan, L., Isola, P., Chang, H., and Krishnan, D. (2024). Stablerep: Synthetic images from text-to-image models make strong visual representation learners. *Advances in Neural Information Processing Systems*, 36.
- Van Horn, G., Mac Aodha, O., Song, Y., Cui, Y., Sun, C., Shepard, A., Adam, H., Perona, P., and Belongie, S. (2018). The inaturalist species classification and detection dataset. In *Proceedings of the IEEE conference on computer vision and pattern recognition*, pages 8769–8778.
- You, Y., Gitman, I., and Ginsburg, B. (2017). Large batch training of convolutional networks. *arXiv preprint arXiv:1708.03888*.
- Zbontar, J., Jing, L., Misra, I., LeCun, Y., and Deny, S. (2021). Barlow twins: Self-supervised learning via redundancy reduction. In *International Conference on Machine Learning*, pages 12310–12320. PMLR.
- Zhang, C., Barbano, R., and Jin, B. (2021). Conditional variational autoencoder for learned image reconstruction. *Computation*, 9(11):114.
- Zhou, B., Lapedriza, A., Khosla, A., Oliva, A., and Torralba, A. (2017). Places: A 10 million image database for scene recognition. *IEEE Transactions on Pattern Analysis and Machine Intelligence*.
- Zhou, J., Wei, C., Wang, H., Shen, W., Xie, C., Yuille, A., and Kong, T. (2021). ibot: Image bert pre-training with online tokenizer. *arXiv preprint arXiv:2111.07832*.

## A Implementation details

### A.1 Standard SSL augmentations

We follow the default standard augmentation settings for each joint embedding SSL algorithm provided in the solo-learn library (Da Costa et al., 2022). These augmentations can be symmetric or asymmetric across the two views of these algorithms. The parameters of these symmetric and asymmetric standard augmentations are provided in Tables 4 and 5, respectively. Additionally, to perform ablation studies for **RQ4** in Section 4.2, we experiment with an extra random crop augmentation, where only crop and flip augmentations are applied as standard augmentations.

Table 4: The augmentation parameter values for SimCLR and MoCo are symmetric across both views.

	Parameter	SimCLR Standard	SimCLR Random Crop	MoCo Standard
Crop	Min Scale	0.08	0.08	0.08
	Max Scale	1.0	1.0	1.0
Color Jitter	Prob	0.8	0.0	0.8
	Brightness	0.8	-	0.4
	Contrast	0.8	-	0.4
	Saturation	0.8	-	0.4
	Hue	0.2	-	0.1
Gray Scale	Prob	0.2	0.0	0.2
Gaussian Blur	Prob	0.5	0.0	0.5
Solarization	Prob	0.0	0.0	0.0
Horizontal Flip	Prob	0.5	0.5	0.5

Table 5: The augmentation parameter values for BYOL, SimSiam, and Barlow Twins. Note that some entries are asymmetric across the two views. Such numbers are shown as A/B.

	Parameter	BYOL Standard	SimSiam Standard	Barlow Twins Standard
Crop	Min Scale	0.08	0.08	0.08
	Max Scale	1.0	1.0	1.0
Color Jitter	Prob	0.8	0.8	0.8
	Brightness	0.4	0.4	0.4
	Contrast	0.4	0.4	0.4
	Saturation	0.2	0.2	0.2
	Hue	0.1	0.1	0.1
Gray Scale	Prob	0.2	0.2	0.2
Gaussian Blur	Prob	1.0 / 0.1	1.0 / 0.1	1.0 / 0.1
Solarization	Prob	0.0 / 0.2	0.0 / 0.2	0.0 / 0.2
Horizontal Flip	Prob	0.5	0.5	0.5

## A.2 SSL methods training

While we follow the default settings for MoCo, SimSiam, and Barlow Twins provided in the solo-learn library (Da Costa et al., 2022), we increase the batch size and decrease the learning rate parameters in SimCLR and BYOL based on their original papers (Chen et al., 2020; Grill et al., 2020), as this yields better performance compared to the solo-learn settings. We also use the learning rate scaling rule:  $lr = base\_lr \times batch\_size/256$ . We present the training details in Tables 6 and 7.

Table 6: SSL pretraining setting for SimCLR, MoCo and BYOL.

Config	SimCLR	MoCo	BYOL
Optimizer	LARS	SGD	LARS
Base lr	0.3	0.3	0.2
Weight decay	1e-6	3e-5	15e-7
Batch size	256	64	256
Learning rate schedule	Cosine decay	Cosine decay	Cosine decay
Warmup epochs	10	10	10
Backbone	Resnet50	Resnet50	Resnet50
Base momentum backbone	NA	0.99	0.99
Final momentum backbone	NA	0.999	1.0
Projector hidden dimension	4096	2048	4096
Projector output dimension	512	256	256
Predictor hidden dimension	NA	NA	4096
Queue size	NA	65536	NA
Temperature for contrastive loss	0.2	0.2	NA

Table 7: SSL pretraining setting for SimSiam and Barlow Twins.

Config	SimSiam	Barlow Twins
Optimizer	SGD	LARS
Base lr	0.5	0.8
Weight decay	1e-5	1.5e-6
Batch size	64	64
Learning rate schedule	Cosine decay	Cosine decay
Warmup epochs	10	10
Backbone	Resnet50	Resnet50
Projector hidden dimension	4096	4096
Projector output dimension	4096	4096
Predictor hidden dimension	512	NA
Cross-covariance matrix off-diagonal scaling factor	NA	0.0051
Loss scaling factor	NA	0.048

## A.3 Linear probing

For evaluation, we adhere to the linear probing protocol of prior studies, which involves training a linear classifier on the output of the frozen encoder for both in-distribution and out-of-distribution downstream tasks. Since the LARS optimizer (You et al., 2017) has been shown to yield better results (Chen and He, 2021), we have chosen to use it as our optimizer. Additionally, it is generally observed that regularization, such as weight decay, can hurt performance. Therefore, we have set the weight decay to 0. We present the linear probing details in Table 8.

## B Complimentary results

In this section, we provide complimentary results for the experiments presented in Section 4.2 of our manuscript. Tables 9 and 10 show the Top-1 and Top-5 accuracy results for experiments related to **RQ1**. Table 11 present the Top-1 and Top-5 accuracy results for experiments associated with **RQ2**. Table 12 shows the Top-1 and Top-5 accuracy results for experiments related to **RQ4**.

Table 8: Linear probing setting for downstream evaluation.

Config	Linear Probing
Optimizer	LARS
Base lr	0.1
Weight decay	0.0
Batch size	512
Learning rate schedule	Cosine decay
Warmup epochs	0

Table 9: Top-1/Top-5 accuracy (%) of linear probing for the baseline (only the standard augmentations) and the generative augmentation on ImageNet.

	SimCLR	MoCo	BYOL	SimSiam	Barlow Twins
Baseline	61.84 / 84.00	60.23 / 82.90	62.20 / 84.04	65.52 / 86.88	67.74 / 87.99
ICGAN	62.92 / 85.05	65.84 / 86.79	65.83 / 86.73	65.53 / 86.21	66.24 / 86.74
Stable Diff	68.11 / 88.86	70.25 / 90.26	69.11 / 89.62	70.84 / 90.07	70.49 / 89.61

Table 10: Top-1/Top-5 accuracy (%) results of linear evaluation on several datasets with different augmentation strategies.

		Food101	CIFAR10	CIFAR100	Places365	iNaturalist
SimCLR	Baseline	58.03 / 83.17	61.74 / 95.73	36.88 / 66.92	46.11 / 77.42	20.17 / 36.88
	ICGAN	57.42 / 81.98	61.92 / 96.16	39.45 / 69.02	45.75 / 76.94	20.25 / 37.47
	Stable Diff	61.78 / 85.86	63.19 / 95.74	39.60 / 70.17	48.40 / 79.51	24.08 / 43.26
MoCo	Baseline	54.50 / 80.21	58.17 / 95.43	34.28 / 64.74	45.70 / 76.62	16.52 / 31.70
	ICGAN	59.92 / 84.01	64.48 / 96.55	40.57 / 71.20	47.69 / 78.60	21.90 / 40.34
	Stable Diff	62.79 / 86.65	64.62 / 96.86	41.33 / 71.89	49.26 / 80.49	25.20 / 45.30
BYOL	Baseline	54.14 / 80.07	55.34 / 94.26	28.70 / 57.82	46.93 / 77.57	6.91 / 21.68
	ICGAN	53.35 / 79.09	60.20 / 95.52	35.17 / 65.59	46.84 / 77.74	8.96 / 19.48
	Stable Diff	55.22 / 80.97	60.30 / 95.83	36.24 / 67.17	47.71 / 79.42	9.96 / 15.84
SimSiam	Baseline	60.71 / 84.65	61.93 / 96.08	37.69 / 67.89	48.78 / 79.64	22.07 / 40.46
	ICGAN	61.06 / 84.37	63.68 / 96.50	38.85 / 69.37	47.41 / 78.25	23.13 / 41.80
	Stable Diff	67.97 / 89.43	64.38 / 96.68	41.31 / 71.22	49.95 / 81.22	31.47 / 65.03
Barlow Twins	Baseline	66.71 / 88.54	65.49 / 96.76	41.19 / 71.34	49.47 / 80.55	27.99 / 47.51
	ICGAN	64.98 / 86.92	64.95 / 96.35	41.52 / 71.70	47.98 / 78.92	25.86 / 45.35
	Stable Diff	68.62 / 89.58	65.21 / 96.68	41.91 / 71.91	49.66 / 80.74	31.14 / 52.07

## C Generative augmentation samples

Fig. 5 illustrates augmentations generated using Stable Diffusion, and Fig. 6 shows augmentations generated using ICGAN. Stable Diffusion is trained on image-text data using classifier-free guidance. In our approach, we condition it solely on the representation of the input image to generate various augmentations. On the other hand, ICGAN is a conditional GAN where the goal of its generator is to produce realistic images similar to the neighbors of each given instance. In ICGAN, images in the same neighborhood may belong to different classes. Therefore, we expect to see instances that may not be from the same class but carry a close representation to the input image.

Table 11: Top-1/Top-5 accuracy (%) of different probability values of applying the generative augmentation to one view or both views, measured on the ImageNet validation set.

	Probability	Imagenet	
		One View	Both Views
SimCLR	0	61.84 / 84.00	61.84 / 84.00
	0.25	66.01 / 88.42	67.26 / 88.11
	0.5	67.62 / 88.92	68.12 / 88.76
	0.75	68.11 / 89.01	67.34 / 88.35
	1.0	68.11 / 88.86	62.11 / 84.41

Table 12: Top-1/Top-5 accuracy (%) of applying different augmentation strategies, measured on the ImageNet validation set.

	Augmentation Strategy	Imagenet
SimCLR	Only standard	61.84 / 84.00
	Only generative	63.80 / 86.00
	Generative & Random Crop	67.15 / 88.22
	Generative & standard	68.11 / 88.86

## D Computation

**Offline generation:** Since generating augmentations on the fly would be time-consuming, we pre-generated augmented instances for the training split of ImageNet, which consists of approximately 1.2 million images. Using Stable Diffusion and ICGAN separately, we ran 10 parallel processes for each model on A100 GPUs, with each process generating one augmented sample per image (resulting in 10 samples in total for each method). Using Stable unCLIP source code<sup>1</sup>, each round of generation over the entire ImageNet took  $\sim 178$  hours. In contrast, ICGAN was four times faster, taking  $\sim 40$  hours to iterate over the entire ImageNet dataset.

**SSL pretraining:** Since we pre-generated augmented samples, during training, we randomly selected one of the 10 samples for each image and applied the appropriate standard augmentation. This process allowed our training time to be equivalent to any other SSL training. We pretrained each SSL method on 4 A40 GPUs, with each run taking  $\sim 34$  hours. It is worth noting that loading ImageNet was our main bottleneck. By using the DALI<sup>2</sup> dataloader, we reduced the training time by almost half.

**Linear Probing:** Computation time for linear probing is highly dependent on the size of the dataset. Using 4 T4v2 GPUs, it took  $\sim 14$  hours for ImageNet,  $\sim 10$  minutes for CIFAR10,  $\sim 10$  minutes for CIFAR100,  $\sim 10$  hours for Places365 and  $\sim 10$  hours for iNaturalist.

<sup>1</sup>[https://huggingface.co/docs/diffusers/en/api/pipelines/stable\\_unclip](https://huggingface.co/docs/diffusers/en/api/pipelines/stable_unclip)

<sup>2</sup>[https://docs.nvidia.com/deeplearning/dali/user-guide/docs/examples/frameworks/pytorch/pytorch-basic\\_example.html](https://docs.nvidia.com/deeplearning/dali/user-guide/docs/examples/frameworks/pytorch/pytorch-basic_example.html)



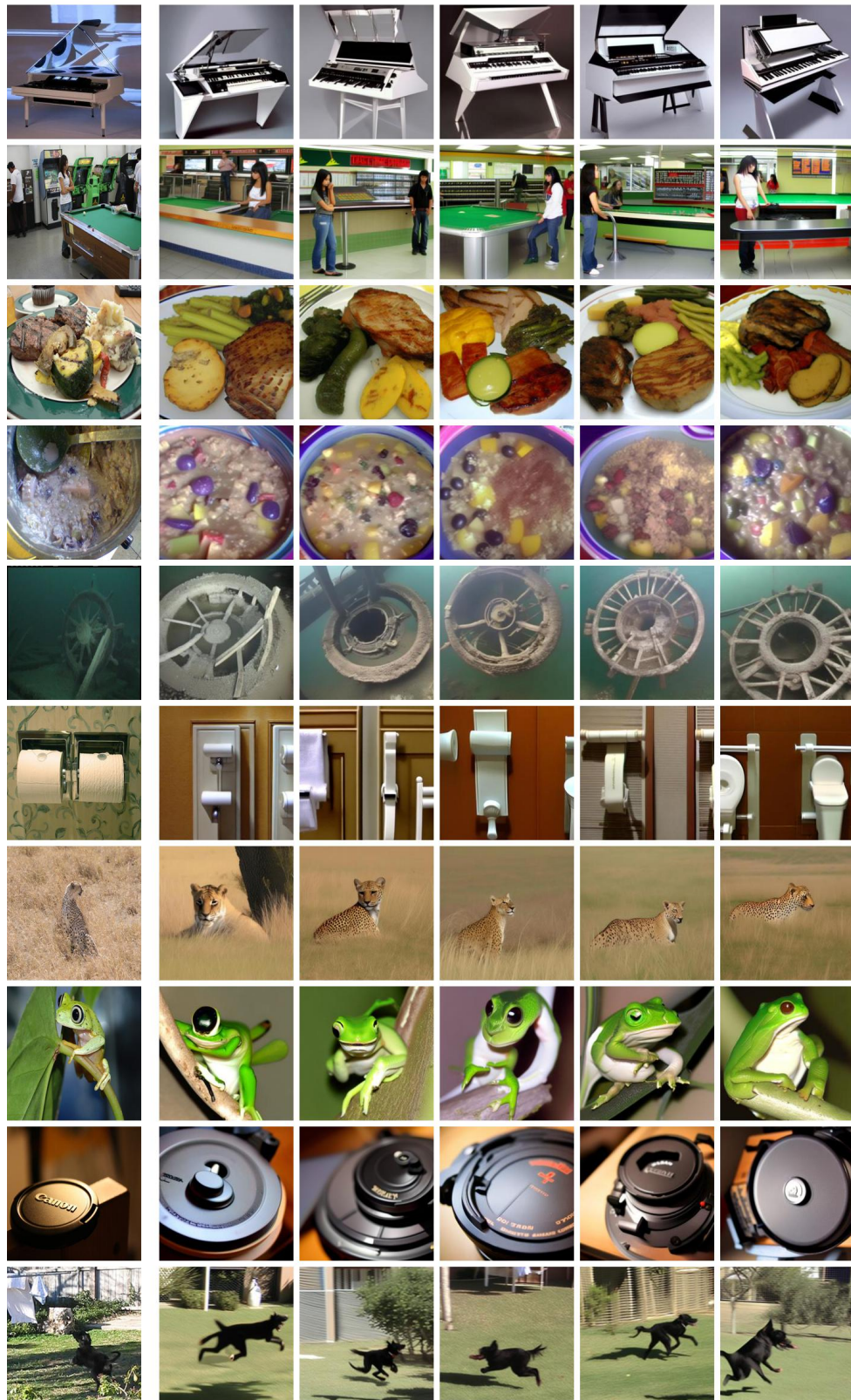


Figure 5: Augmentations generated by Stable Diffusion. The first column shows the original images, and the other columns show the generated augmentations.

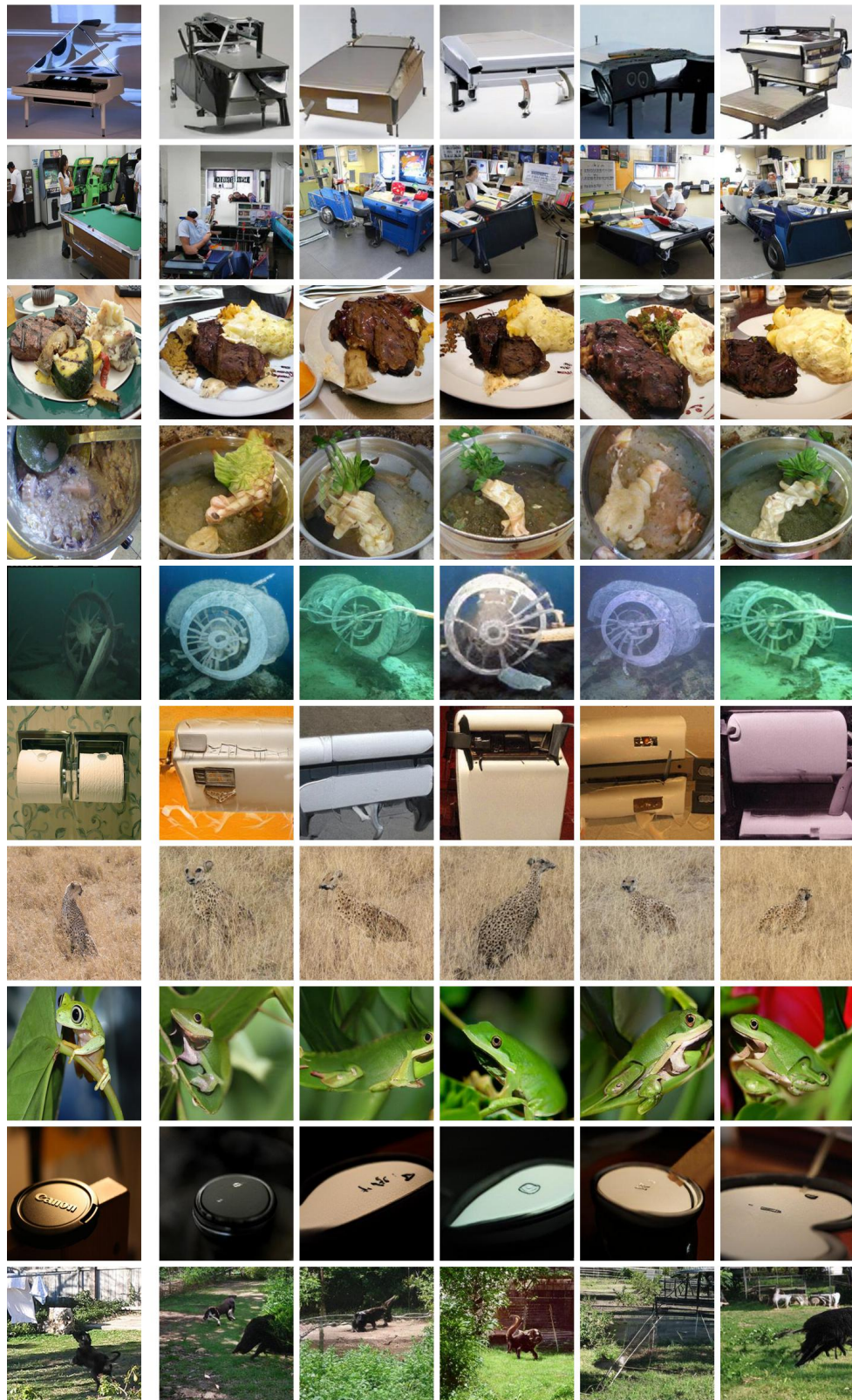


Figure 6: Augmentations generated by ICGAN. The first column shows the original images, and the other columns show the generated augmentations.